Hydrogeol J (2017) 25:877–894
DOI 10.1007/s10040-017-1560-x

TECHNICAL NOTE

A numerical investigation of pumping-test responses from contiguous aquifers

Silvain Rafini[1] · **Romain Chesnaux**[1] · **Anouck Ferroud**[1]

Received: 3 December 2015 / Accepted: 20 February 2017 / Published online: 9 March 2017

Abstract Adequate groundwater management requires models capable of representing the heterogeneous nature of aquifers. A key point is the theoretical knowledge of flow behaviour in various heterogeneous archetypal conditions, using analytically or numerically based models. This study numerically investigates transient pressure transfers between linearly contiguous homogeneous domains with non-equal hydraulic properties, optionally separated by a conductive fault. Responses to pumping are analysed in terms of time-variant flow dimension, n. Two radial stages are predicted (n: 2 – 2) with a positive or negative vertical offset depending of the transmissivity ratio between domains. A transitional $n = 4$ segment occurs when the non-pumped domain is more transmissive (n: 2 – 4 – 2), and a fractional flow segment occurs when the interface is a fault (n: 2 – 4 – 1.5 – 2). The hydrodynamics are generally governed by the transmissivity ratio; the storativity ratio impact is limited. The drawdown log-derivative late stabilization, recorded at any well, does not tend to reflect the local transmissivity but rather the higher transmissivity region, possibly distant and blind, as it predominantly supplies groundwater to the well. This study provides insights on the behaviour of non-uniform aquifers and on theoretical responses that can aid practitioners to detect such conditions in nature.

✉ Romain Chesnaux
romain_chesnaux@uqac.ca

[1] Research Group R2Eau, Centre d'études sur les ressources minérales, Université du Québec à Chicoutimi, 555, boulevard de l'Université, Chicoutimi, Québec, Canada G7H 2B1

Keywords Pumping tests · Heterogeneity · Hydraulic properties · Derivative analysis · Flow dimension

Introduction

Natural aquifers are essentially heterogeneous systems. Identifying hydraulic heterogeneities and anticipating their impact on groundwater flow is a fundamental and most important task given to hydrogeology researchers and practitioners. To this end, pumping tests constitute an adequate approach only if interpretative models are able to account for the heterogeneity of flow. Eighty years ago, the ground-breaking Theis (1935) model, later referred to as the *infinite acting radial flow* model, provided an analytical solution to the hyperbolic transient diffusivity problem by assuming a perfectly homogeneous flow configuration. By its very nature, this highest degree of idealization of aquifers is unable to render any heterogeneity of flow occurring in real aquifers. Critics of the model have cited its lack of realism, which leads to overly gross and approximate aquifer interpretations (Renard 2005; Renard et al. 2008; Pechstein et al. 2016). For practical and contextual reasons, this model has been the one most often used in hydrogeology applications without much assessment of the degree to which it diverges from reality. In contrast, decades of active research in the petroleum and hydrogeology fields have yielded several advances for modelling heterogeneous flow. The derivative analysis (Tiab and Kumar 1980; Bourdet et al. 1983, 1989; Spane 1993; Spane and Wurstner 1993; Beauheim et al. 2004; Samani et al. 2006; Dewandel et al. 2011; Avci et al. 2013; Xiao and Xu 2014; Sun et al. 2015) is frequently referred to as one of the most significant breakthroughs in pumping test analysis (e.g., Issaka and Ambastha 1999; Renard et al. 2008; Hammond and Field 2014). The central idea consists in deciphering the reservoir

response to pumping tests by identifying the various types of flow regimes that are recorded, based on the shape of the drawdown log-derivative time series. Real data are compared to a reference panel of theoretical behaviors that have been established as corresponding to various conceptual flow models (Verweij 1995). These conceptual flow models are idealized models of aquifers which provide hydrogeologists with a range of archetypal frameworks used to interpret and describe real-world conditions that are more complex than basic idealized models. A first generation of these models is (semi-)analytical solutions of the diffusivity equation, assuming specific hydraulic and geometrical aquifer conditions. For mathematical suitability, strong postulates must commonly be made on the geometry of transient flow to reduce the diffusivity problem—a second-order partial differential equation, to a solvable form. Purely numerical approaches used in an experimental mode provide a second generation of conceptual models, predicting drawdown responses in two-dimensional (2D) or three-dimensional (3D), analytically unsolvable, heterogeneous flow configurations (e.g., Bourdet 2002). In such an approach, serial flow simulations into synthetic domains are processed to assess the sensitivity of the drawdown responses to every hydraulic and geometrical input parameter, into a given conceptual configuration (e.g., Rafini and Larocque 2009, 2012). A second breakthrough in pumping test analysis was the flow dimension theory (Barker 1988). It offered significant new perspectives in modelling hydraulic behavior by generalizing the conception of flow regimes to drawdown log-rates either increasing with time (flow dimension less than two) or decreasing with time (flow dimension greater than two), while previously published models accounted for drawdown log-rates constant or varying with time following specific coefficients 0.25, ±0.5 or ±1. A constant drawdown log-rate such as described by Theis (1935), corresponds to the radial flow regime; such a regime is characterized by a flow dimension equal to two. Henceforth, to justify appropriate use of the Theis or Cooper-Jacob (1946) models, prior identification of such flow dimension conditions would theoretically be required; however, this is rarely if ever done in practice. Both the derivative and the flow dimension approaches have this in common, that they recognize the existence in nature of various types of flow regimes. Based on this recognition, and using recently developed approaches, it is now possible to select appropriate conceptual flow models by identifying the time-sequences of flow regimes observed during a pumping test. These concepts are the foundation for the interpretative framework proposed in this study.

The manner with which natural heterogeneities are hydraulically represented in commonly used conceptual models greatly depends on their size in relation to that of the investigated domain. In natural aquifers, heterogeneities governing hydraulic properties occur at various scales, from the very small (cm) grain or crystal arrangements, to commonly found networks with characteristic metric fracture lengths, to large-scale (km) features such as lithological spatial variations or regional structures where groundwater transfers occur primarily through faults, or to cross-connected aquifers (Chesnaux et al. 2012). It is of particular interest that in pumping-test conditions, the relative influence of micro-, meso-, and macro-scale heterogeneities on the drawdown response is time-variant as the scale of the investigation grows over time. Smaller-scale heterogeneities may typically be considered as fields, and may be adequately described using statistical functions; however when the investigation scale grows larger than the typical size of a single heterogeneity, usually after a very short pumping time, these fields tend to behave like homogenous media, with properties averaging the distribution function (e.g., Meier et al. 1998). Induced flow regimes will be radial, except when the distribution is scale-invariant (Cello et al. 2009). Such fields are typically well represented using stochastic hydraulic models. Conversely, larger heterogeneities that occur on a scale ranging from decameters to several kilometers must, in most pumping test cases, be represented as independent hydraulic domains influencing the macro-scale behavior during restricted time periods, i.e., when the investigation scale is of a magnitude which is comparable to the scale of the heterogeneity. These larger heterogeneities can often be modelled deterministically because only a small number of them may exert a significant impact on the flow field at any given time. Thus, the objective in this study is not to simulate stochastic heterogeneity fields but to deterministically investigate the hydrodynamic impact of specific types of large-scale heterogeneities, producing complex non-radial flow geometries. The evolving influence of such heterogeneities on the flow regime over time tends to generate convoluted responses to pumping tests, with time-variant flow regimes and inconstant drawdown log-rates.

Large-scale heterogeneous flow may result from the coexistence of several flow domains in the aquifer, each with different hydraulic properties. Indeed, in many real-life situations, the transmissivity and storativity may have different magnitudes in some domains (Rushton 2003). The assumption that hydraulic parameters are constant in the entire space located between the pumped borehole and the farthest limit of the field where pumping no longer exerts an influence may lead to false conceptual and quantitative interpretations. The hydrodynamic behavior of such composite systems has been studied analytically, assuming a radially symmetry of hydraulic domains (Barker and Herbert 1982; Bourdet et al. 1983; Butler 1988; Ambastha 1989; Oliver 1990, 1993; Roberts et al. 1996; Issaka and Ambastha 1999; Jordan and Mattar 2000). These models, referred to as *patchy aquifers* or *composite domains*, are intended to investigate pumping test responses when the local region in the vicinity of the pumped borehole is not representative of the reservoir's general hydraulic properties. For analytical suitability, the *patch* is

represented by a cylinder whose center is embodied by the pumping well. The predicted drawdown response of a linear interface between the two domains is more complex due to the fact that induced flow geometry is non-uniform in a 2D space. Such a configuration is also referred to as a *linear strip* or *multi-strip* reservoir. Guo et al. (2012) proposed an analytical solution for a three-region channel-aquifer combined with a dual porosity model. Flow restriction into a corridor makes it possible to process the interferences between flow domains as mathematically suitable one-dimensional (1D) problems. They obtained successive linear flow regimes before and after lateral domains were reached by the depressurization front. Ambastha et al. (1989) proposed an analytical solution for a "two-region reservoir" separated by a communicating fault, and for a strip aquifer, with emphasis on skin effects; however, the study focussed on the latter configuration with little development on the former, and the flow into the fault is not explicitly modeled. This nonintersecting finite-conductivity fault problem was later analytically approached by Abbaszadeh and Cinco-Ley (1995). These authors postulated that the problem could be reduced to three solvable problems, independent, radial and linear: (1) linear flow into the fault; (2) flows into the two embedding semi-infinite reservoirs are converted into infinite-acting flow problems by mirror-imaging them against the fault plane. The equality of pressure and fluxes is finally imposed at the domain interfaces in order to preserve hydraulic continuity. Butler and Liu (1991) developed a semi-analytical solution for a two-region aquifer split by a more transmissive strip which, under certain conditions (small transversal extent), tends to behave like a fault. Interestingly, although they used different modeling approaches, Abbaszadeh and Cinco-Ley (1995) and Butler and Liu (1991) arrived at conclusions that converge, in the sense that they predict a specific time-period where the aquifer response to pumping is predominantly governed by the properties of the nonintersecting fault or strip, namely where the flow dimension is equal to 1.5 (equivalent to the bilinear flow regime, see Rafini and Larocque 2009). Dewandel et al. (2014) submitted an analytical multi-domain model for "T" shape aquifers, which are formed by a deep and narrow region (representing a vertical fault) surrounded by two shallower and less transmissive domains. The interferences of transient depressurization into the fault and adjacent flow domains produce time-variant drawdown regimes that are analytically approximated as several infinite series of well-image functions.

This study numerically investigates the transient behaviour of aquifers composed of two laterally juxtaposed flow domains with differing hydraulic properties where the non-pumped domain may be either more transmissive or less transmissive then the pumped one. A method is proposed which predicts a singular theoretical response, in the form of a flow-dimension-sequence signature, which makes it possible to identify such aquifers in pumping test contexts. Classic analytical solutions account for the flow behavior of juxtaposed hydraulic domains in extreme hydraulic conditions, including the impermeable barrier (i.e., non-conductive boundary) and constant-head boundary solutions (i.e., infinitely conductive). The numerical experiments described here investigate intermediate cases in which both domains have finite conductivities and the interface is non-impermeable. The pressure transfers between both domains are deeply investigated as well as their time-variant relative contribution in supplying groundwater to the pumping well. Several cases are considered, with and without the occurrence of a fault at the interface between both domains. Cases where the non-pumped domain is respectively more transmissive and less transmissive than the pumped domain will hereafter be referred to as *leaky* and *non-leaky* cases. These two limiting cases deeply diverge from a hydrodynamic standpoint in that the domain which is predominantly supplying the well is the pumped domain or the non-pumped domain. The term *leaky* is borrowed from Hantush (1960) because the conceptual configuration to which this paper refers is a horizontal equivalent of the classic leaky aquifer model: in both cases, the pumped groundwater is supplied by a distant reservoir that is juxtaposed, either horizontally or vertically, to a less transmissive pumped aquifer; however, both problems are drastically different from a hydrodynamic perspective (i.e., geometry of leaky flow).

Materials and methods

The numerical simulations are performed using the HydroGeoSphere code, which is a three-dimensional finite-element code that has been used by numerous hydrogeology researchers (Brunner and Simmons 2012). Constitutive diffusion equations are solved using the control volume method with a fully implicit time discretization. The spatial discretization uses orthogonal tridimensional prisms of various sizes that are adjusted to anticipated drawdown variations. Hydraulic continuity between sub-domains (well/matrix or matrix/matrix) is implicitly ensured by superposing respective flow contributions at the interface nodes.

The inner boundary conditions are those of a pumping test. The wellbore is vertical, unidimensional and entirely cross-cuts the aquifer. The source has no storage and a screen radius of 0.05 m. The pumping rate, Q, is equal to 4.17×10^{-4} m^3 s^{-1} or 1,500 L h^{-1}. The upper and lower boundaries are impermeable. The initial head is uniform over the entire domain and is equal to the constant-head values at the lateral boundaries. Time sampling is logarithmic and contains approximately 100 steps, beginning at 10^{-2} and ending at approximately 10^9 seconds.

The flow domain is designed to be artificially large (4×10^5 by 4×10^5 by 42 m), the duration of the simulated pumping

tests is intentionally long (10^9 and 10^{11} s), while the distance, d, between the pumping well and the interface, is set at 2 m. These settings were designed for numerical experiment suitability, i.e., to "scan" a wide spectrum of parameter combinations to fully constrain the behavior of the system, without changing the model's geometry. Explicitly, to properly constrain the impact of a given parameter, it is necessary to perform numerous simulations while changing only this parameter, from the lower limiting case to the upper limiting case. Accordingly, the simulations were configured to optimize the visibility of successive flow regimes without changing other input parameters, even when covering a large panel of parameter combinations (e.g., aquifers transmissivities, T_m, ratios). The implications of the modelling settings are addressed in the section 'Discussion', notably on the matter of using the results in real-world conditions. First, the technical note presents the case of laterally juxtaposed flow domains with no fault at the interface. Then, the effect of a finite-conductivity fault on transient flow interactions between the two domains is analysed. Such disposition of a fault between two distinct lithological domains is a widespread tectonic situation, since the fundamental characteristic of a fault is that it splits and offsets two contiguous units. The aquifer thicknesses, b, are set to 42 m. The interface between the two flow domains is vertical. Lateral boundaries oriented parallel to the Oy axis possess constant heads equal to 80 m, whereas those oriented parallel to the Ox axis are no-flow boundaries (Fig. 1). When present, the fault is vertical, 0.3 m wide and entirely crosscuts the aquifer. It is considered as a tabular vertical thin aquifer in itself, which allows for transient flow to be resolved in a similar fashion to a porous medium. Thus, the fault is viewed as a Darcian medium rather than a Poiseuille fracture. The Poiseuille model is considered inadequate to represent macro-scale faults, which are much thicker than infra-meter-scale fractures and contain material-filled core rather than void space. The hydraulic properties are isotropic in the entire flow domain. The drawdown response examination focuses on time periods prior to reaching the lateral boundaries. The size of the mesh in the vicinity of the pumping well is 0.05 m, which progressively increases toward the boundaries. No vertical flows are generated from these configurations. Therefore, the vertical discretization is strongly restricted (three cells), for computing purposes. Only one flow domain is pumped (domain A); the non-pumped flow domain (domain B) can be variably conductive, and hence may or may not produce leakage from domain B to domain A. Finally, numerous simulations are performed to produce a systematic analysis of the effect of each hydraulic input parameter on the macroscopic response rendered at the pumping well. These series of simulations are designed to achieve a general flow behavior in which the sensitivity of every parameter is known.

Results from numerical simulations are analysed in terms of drawdown log-derivative $ds/d\log(t)$ and of flow dimension n that is calculated following the definition of Barker (1988), $n = 2 - 2(p)$, where p is the slope of the log-derivative series. This equation of n postulates an asymptotic approximation that is, from a practical standpoint, valid after a very short pumping time at the pumping well.

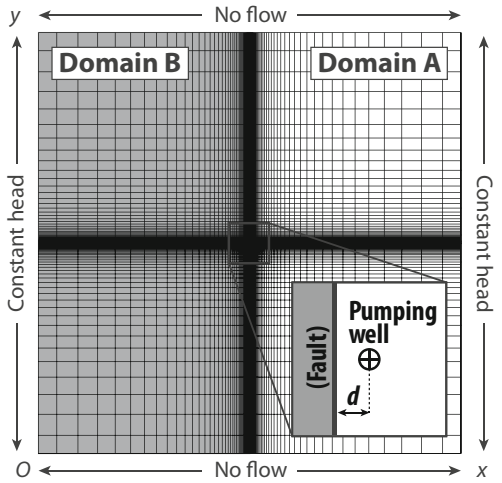

Fig. 1 Configuration used for the numerical flow simulations in laterally juxtaposed flow domains. The grid corresponds to the spatial discretization. Two cases are considered depending upon the occurrence of a fault at the interface between domains *A* and *B*

Results

Contiguous aquifers with unfaulted interface

Influence of the conductivity ratio

The pumping well drawdown responses obtained from flow simulations with varying conductivity of the non-pumped domain, K_{mB}, are presented in Fig. 2. A series of simulations was performed to assess the influence of K_{mB} being lower or higher than the pumped domain conductivity, K_{mA}, by incrementally changing K_{mB}, starting with $K_{mA} = K_{mB}$. The signals are composed of three successive flow regimes: (1) early radial flow corresponding to the normal diffusion into domain A before domain B is reached; (2) a transitional period marked by a characteristic derivative slope of $p = -1$ ($n = 4$); and (3) late radial flow corresponding to a simultaneous diffusion into both domains. The elevation, a, of the plateau formed during the radial flow regime is an inverse function of the conductivity. This function is simply derived using the Cooper-Jacob's model: $a = 2.3Q/4\pi T$, where T is the transmissivity and Q is the pumping rate. Here, the late radial plateau elevation, a_{r2}, displayed in Fig. 3, provides an apparent conductivity, K_{app}. The positive vertical offset of this plateau between the early and late radial stages is equal to log (2) when $K_{mB} << K_{mA}$ (i.e., the non-leaky case) because $K_{app} = K_{mA}/2$. This results in the classical impermeable boundary model (i.e., doubling the

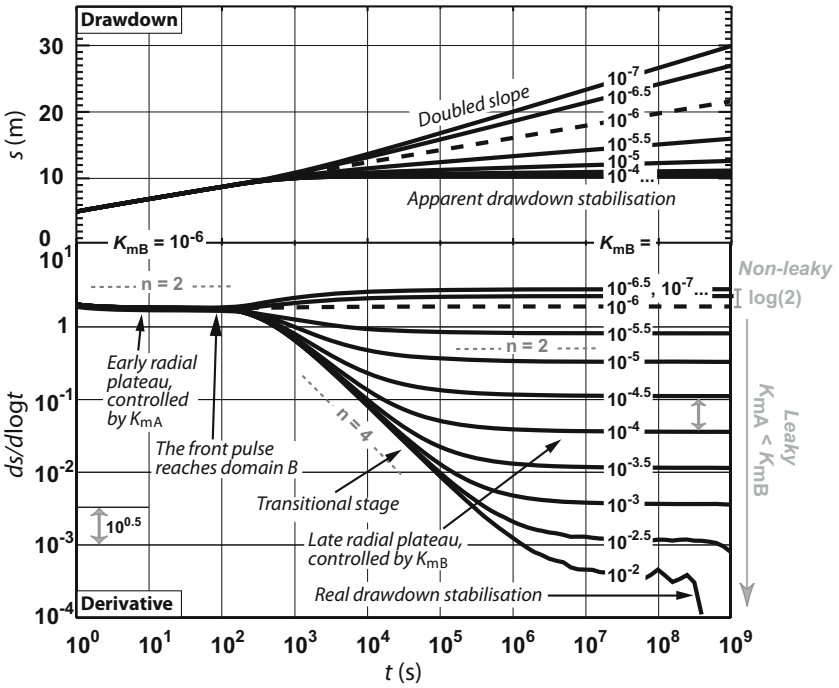

Fig. 2 Simulated drawdown and drawdown log-derivative obtained from unfaulted laterally juxtaposed flow domains with different values of conductivity ratios. *n* indicates the successive flow dimensions. A series of simulations are performed with identical parameters except for the conductivity of the non-pumped domain B, K_{mB}, which varies by increments of $10^{0.5}$ m s^{-1}, beginning with $K_{mA} = K_{mB}$ (*dotted signal*). Other parameters are $K_{mA} = 10^{-6}$ m s^{-1}; $S_{s\_mA} = 10^{-4}$ m^{-1}; $S_{s\_mB} = 10^{-4}$ m^{-1}; $d = 2$ m; and $Q = 4.16 \times 10^{-4}$ m^3 s^{-1}

drawdown slope on conventional semi-log plots). However, when $K_{mB} >> K_{mA}$ (i.e., leaky cases), the vertical offset is negative and proportional to K_{mB} in such manner that $K_{app} = K_{mB}/2$; hence, when the non-pumped, more transmissive aquifer starts being depressurized, both the drawdown rate and its log-derivative drop. It is worth noting that, on a classic semi-log plot, this drop produces an apparent stabilization that is likely misinterpreted as the attainment of a recharge boundary (Fig. 2). Finally, these observations lead to the conclusion that the apparent conductivity is equal, in both configurations, to half the highest conductivity.

A series of simulations with varying K_{mB} and K_{mA} values achieved the relationship $K_{app} = (K_{mB} + K_{mA})/2$, which is shown in Fig. 4. For each of the three lines shown in this figure, the zone in which both conductivities significantly affect K_{app} is represented by the curved portion of the line between the straight portions that correspond to the dominance of either K_{mA} (horizontal straight portion, i.e., K_{mB} is negligible) or K_{mB} (unit slope straight portion, i.e., K_{mA} is negligible). This curved portion is nearly an order of magnitude wide along the K_{mB} axis, which means that the lower

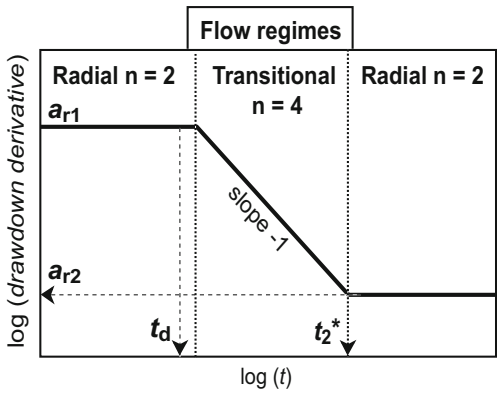

Fig. 3 Schematic illustration of the successive flow regimes predicted in the non-faulted leaky model, and their associated graphical features (see Table 1 for equations)

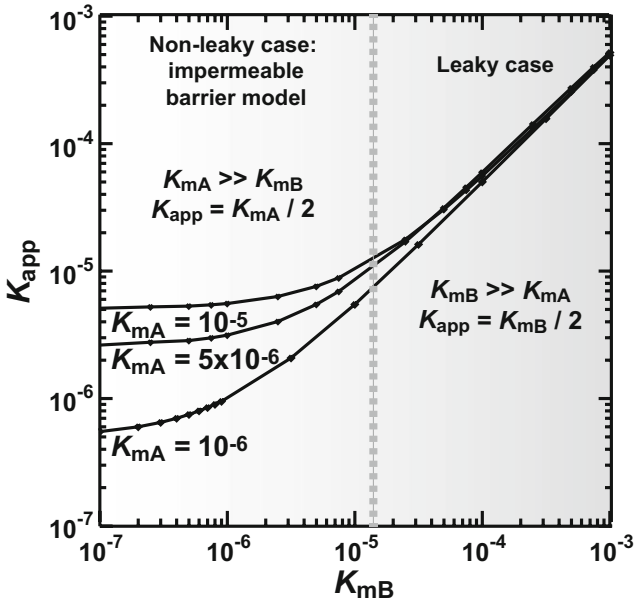

Fig. 4 K_{app} vs K_{mB} exhibiting the two models depending on the K_{mB}/K_{mA} ratio: laterally juxtaposed flow domains models with respectively high and low conductivity of the lateral flow domain (referred to as leaky and non-leaky cases in the text). The low conductivity case is similar to the impermeable barrier model. *Each point* corresponds to a numerical flow simulation

conductivity becomes practically negligible when the conductivity differences between both flow domains exceed half an order of magnitude (i.e., a factor of 3.16), all other parameters being equal.

During the second radial flow regime, the macroscopic behavior of the system, as given by the drawdown response at the pumping well, is controlled by the most conductive flow domain because drawdown propagation in the less conductive domain is slower [$r(t) \sim (K_m)^{0.5}$]. Thus, the portion of the cross-flow area (i.e., the surface of the front of depressurization) in this domain becomes negligible compared with the portion that propagates into the most conductive domain in such a manner that its depressurized volume becomes lower than that of the most conductive domain, as does its contribution to supplying water to the pumping well. This phenomenon is perfectly illustrated in Fig. 5 for the leaky case: the relative groundwater contributions from both domains to the pumping well becomes inverted over time, as the aquifer response becomes controlled by the properties of the non-pumped, and more transmissive, aquifer.

The outward propagation of drawdown into the two half-spaces forms two half front pulses growing at two different rates (Fig. 6). Only the half that propagates into the more conductive domain has a significant effect on the drawdown response at the pumping well during the late radial stage. The response is entirely controlled by the transient growth of the dominant front, whether or not this half front evolves into the flow domain that is directly pumped. In other words, if the non-pumped domain is the most conductive, the properties of the pumped domain have no influence on the drawdown response measured at the pumping well during this late radial stage. Finally, as the effective cross-flow surface growth is restricted to a half space, it takes the shape of a half cylinder, and the transmissive area is half that of an entire cylinder, which explains why the apparent conductivity is half the real conductivity of the most conductive domain.

In the leaky case, the significant portion of the domain supplying the well schematically forms a half cylinder in domain B (Fig. 6b), during the late radial stage; hence, from a hydrodynamic perspective, this can be regarded as an inverted impermeable boundary model (with the pumped domain playing the role of the barrier), albeit the less conductive domain is not actually impermeable. Analytically, the respective drawdown influences of both half fronts at the pumping well can be separately described. Based on the numerical simulation results, these drawdowns can be represented using the superposition of two impermeable-boundary radial solutions: one normal (domain B plays the role of barrier) and one inverted (domain A plays the role of barrier; see Fig. 6). These two solutions correspond to two half front pulses with unequal radii (approximate cylinders), one being largely dominant depending on the respective properties of both domains. The impermeable-boundary solution classically uses an

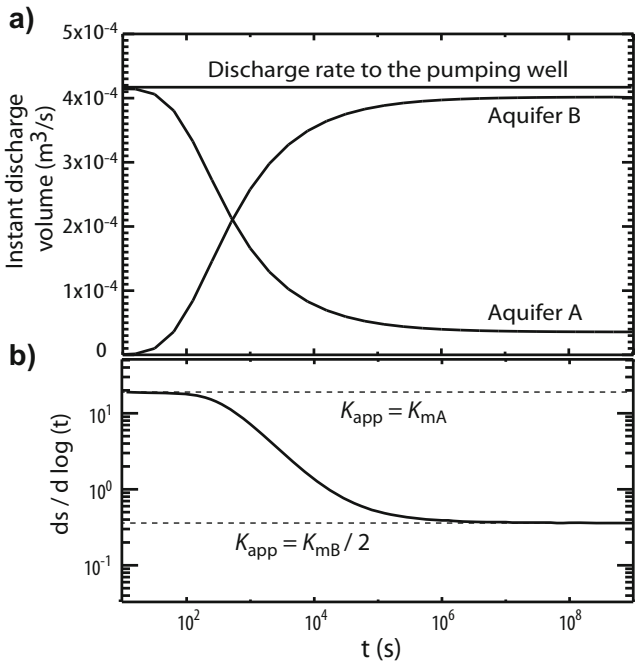

Fig. 5 **a** Evolution of the relative contribution of both domains to the pumping well discharge for the leaky case; **b** associated derivative response. Simulation input parameters are: $K_{mA} = 10^{-7}$ m s^{-1}, $K_{mB} = 10^{-5}$ m s^{-1}, $S_{s\_mA} = S_{s\_mB} = 10^{-5}$ m^{-1}; other conditions are identical to Fig. 2

image-well analysis, which is based on the superposition of a fictitious well that is symmetrically opposite the true well, beyond the barrier. It is theoretically pumped at a rate equal to that of the true well in order to mimic the boundary effect (Ferris 1949; Fenske 1984); thus, the behavior of the system may be represented by four Theis functions: two with K_{mA} and S_{s_mA} properties (normal impermeable-boundary solution with real pumping in domain A and its image in domain B; S_S is specific storage) and two with K_{mB} and S_{s_mB} properties (inverted impermeable-boundary solution with "false pumping" in domain B and its image in domain A). For each couple, one term (pumping or image) would have a distance equal to the well-casing radius and the other a distance equal to $2d$; however, this assumption requires further validation. Separately, the two wells used in this solution can represent some of the flow regimes numerically achieved in this study, including early radial and late impermeable-boundary radial (non-leaky case) conditions; however, the late radial flow regime, or the leaky, inverted impermeable-boundary case (Fig. 6b), cannot be described by a trivial addition of these four terms, nor can a general solution be proposed that includes all flow stages. The reason is that this regime occurs in domain B, while in every case the early radial flow stage occurs in domain A; thus, an analytical solution to this problem requires further work.

Finally, it should be noted that the S_{s_mA}/S_{s_mB} ratio does not impact the shape of the derivative response, since it does

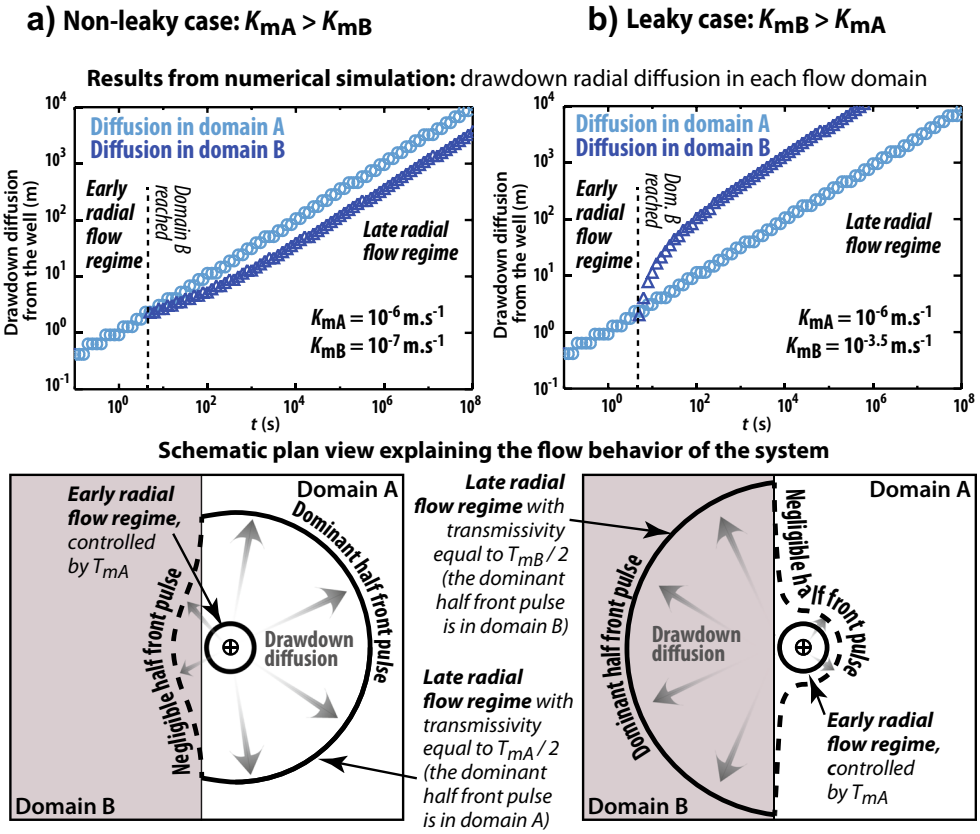

Fig. 6 *Top row*: Drawdown diffusion vs elapsed pumping time obtained from simulations with (*panel a*) $K_{mA} > K_{mB}$ and (*panel b*) $K_{mB} > K_{mA}$. Other parameters are $S_{s\_mA} = S_{s\_mB} = 10^{-4}$ m^{-1}; $Q = 4.16\ 10^{-4}$ m^3.s^{-1}; and $d = 2$ m. *Bottom row:* Schematic views of the front pulse geometries for cases (*panel a*) and (*panel b*) during early and late radial flow stages. The *small crossed circle in the middle* is the pumping well. *Dotted lines* mark the portion of the depressurization front pulse that exerts a negligible influence on the macro-scale response. T_{mA} and T_{mB} are the transmissivities for domains A and B, respectively

not influence the elevations of the plateaus. It only slightly affects the shape of the transition $n = 4$ stage.

Calculation of hydraulic parameters

The diagnostic tool for the unfaulted leaky model is formalized in Fig. 3 and Table 1. The time, t_d, corresponds to the time it takes the front pulse to reach domain B. The solution of the set of three equations (Eqs. 1, 2 and 5 in Table 1) permits the estimation of K_{mA}, K_{mB} and the distance, d, from the pumping well to domain B; however, this equation for t_d, which was proposed by Banton and Bangoy (1999), must be considered a first-order approximation. The form of the equation is correct because it is derived from the normal diffusion law $r^2 = C\,(K/S_s)\,t$, but stating a diffusion coefficient, C, equal to 2.25 is based on the Cooper-Jacob solution (by posing drawdown equal to zero), which is not valid at early pumping times. During this time period, drawdowns are expected to diffuse in a strictly Theissian mode, which is faster due to a coefficient C equal to 4π based on the Theis solution, a value which falls much closer to, if not exactly on, the value derived from the numerical simulations of this study. Moreover, this equation does not account for any delay in the propagation of the front pulse caused by wellbore depressurization and/or skin effects; hence, Eq. (5) likely underestimates (strong wellbore storage or skin effect) or overestimates t_d (C greater than 2.25). This issue remains unresolved and requires further investigation, as it falls outside the scope of this article. In particular, it should be pondered that time-distance scaling relationships may vary with successive, radial and non-radial flow regimes. The formula published by Banton and Bangoy (1999) will be considered acceptable here as a first estimate.

Analysis of observation well data

Simulated drawdown behavior in synthetic observation wells (OW) at various distances from the pumping well are analysed. Specifically, this investigation focuses on the case of interest where the non-pumped domain B is the most conductive and hence predominantly supplies groundwater via the pumped domain A (leaky case). To this end, K_{mB} is set two orders of magnitude higher than K_{mA}.

Figure 7 depicts the derivative responses obtained at OW at various distances from the pumping well. Only OWs located along the axis perpendicular to the interface are displayed, for illustrative purposes. At equal distance from the pumping well, OW located along other directional axes give derivative responses ranging between western and eastern OW along the *Ox* axis. Two plateaux are exhibited, corresponding to the successive predominance of radial flow regimes occurring

Table 1 Algebraic expressions of the graphical features of the models: segment intercepts and critical times

Eq. number	Expression	Graphical feature	Source
1	$a_{r1} = \frac{2.3Q}{4\pi b K_{mA}}$	Early radial plateau elevation	Modified from Cooper and Jacob (1946)
2	$a_{r2} = \frac{2.3Q}{4\pi b\left(\frac{K_{mA}+K_{mB}}{2}\right)}$	Late radial plateau elevation	This study (modified from Cooper and Jacob 1946)
3	$a_f = \frac{2.8Q}{4\pi b T_f^{0.5}\left(S_{s\_m}\frac{K_{mA}+K_{mB}}{2}\right)^{0.25}}$	Intercept of the $n = 1.5$ segments	Modified from Rafini and Larocque (2009)
4	$a_{tr} = \frac{0.21d^2Q}{b\eta_{mA}K_{mA}}$	Intercept of the $n = 4$ segments	This study
5	$t_d = 0.44\frac{d^2}{\eta_{mA}}$	Reaching of the interface	Cooper and Jacob (1946), Banton and Bangoy (1999)
6	$t_2^* = 0.58\frac{d^2}{\eta_{mA}}\frac{K_{mB}}{K_{mA}}$	Intersection time between segments $n = 4$ and late $n = 2$	This study
7	$t_{2AB} = \frac{0.44T_f^2 S_{s\_m}}{\left(\frac{K_{mA}+K_{mB}}{2}\right)^3}$	Intersection time between segments $n = 1.5$ and late $n = 2$	Modified from Rafini and Larocque (2009)
8	$t_1 = \frac{0.11S_f^2}{K_m S_{s\_m}}$	Beginning of the diffusion slow-down in the fault	Modified from Rafini and Larocque (2009)

Note t_2^* was obtained by assuming $K_{mB} >> K_{mA}$, and hence is exclusively valid for the leaky model. S_{s_m} is the bulk specific storage coefficient, which encompasses S_{s_mA} and S_{s_mB}. It is shown that $S_{s\_m} \approx (S_{s\_mA} + S_{s\_mB})/2$. S_f is the fault's storage coefficient. Other parameters are introduced in the text

respectively in domains A and B as explained in the preceding. These two plateaux (early radial plateau and late radial plateau) are visible particularly well on the normalized t/r^2 plot. Due to the short distance (2 m) between the pumping well and the interface, the duration of the early radial plateau is short. OW located at distances less than 2 m behave similarly both on the west and east sides of the pumping well a predictable result, since domain B has not yet been reached. At greater distances, the influence of an early radial flow regime is practically invisible on western OW, while eastern OW display a gradational transition to the late radial plateau elevation.

An unexpected result is that, among the eastern OW, i.e., those located on the side opposite to the interface, drawdown

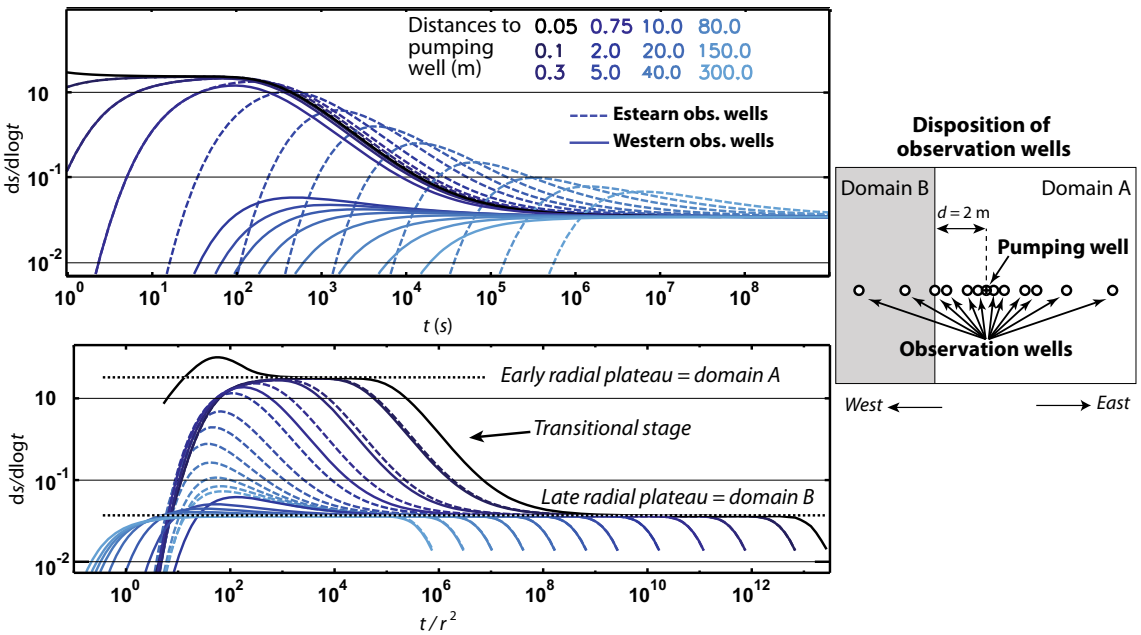

Fig. 7 Simulated drawdown log-derivative obtained from observation wells and the pumping well, in the unfaulted leaky case. The configuration is similar to Fig. 2 results. The pumping well response is shown in *black color* (distance is equal to the casing radius, 0.05 m). Hydraulic parameters are $K_{mA} = 10^{-6}$ m s^{-1}; $K_{mB} = 10^{-4}$ m s^{-1}; $S_{s\_mA} = S_{s\_mB} = 10^{-4}$ m^{-1}; $Q = 4.16 \times 10^{-4}$ m^3 s^{-1}

regimes do not rapidly adjust to the dominant aquifer behavior that is obtained at the pumping well and in the western OW. Indeed, at late time, when the pumping well response clearly shows that a late radial flow regime has settled into the aquifer and dominates its macro-scale hydrodynamics, the drawdown derivative in these distant eastern OW does not merge with this radial regime but rather displays a prolonged gradational transition. This implies that, while the drawdown regime tends to equilibrate over the entire aquifer, the attainment of such homogenous dynamic state is very slow in regions distant from the hydraulic heterogeneity governing the global behavior. This study's results suggest that, over the time scale of a pumping test, the state of equilibrium may not be obtained in distant OW. The greater the distance between the eastern OW and the pumping well and the contrast in conductivity between both aquifers, the later the late radial plateau settles after the transitional stage. This phenomenon may impede its proper identification in real pumping test conditions. This conclusion meets that of Ambastha et al. (1989).

After the transitional stage, drawdown behaviors in all OW are governed by the late radial flow regime. This regime is strictly controlled by the transmissivity of the non-pumped domain B, since domain B is more transmissive, as explained in previous sections. In other words, the transmissivity one would estimate by a classic Cooper-Jacob interpretation of the late radial regime measured in an OW located in domain A *would actually correspond to the transmissivity of domain B* (or more precisely, half of it as explained previously). This counteracts the general belief that the transmissivity measured at an OW is always a proxy to the *T*-field into the area between the OW and the pumping well. Instead, the results indicate that, after late-time stabilization of the derivative, the apparent *T* value actually corresponds to that of the more transmissive region of the aquifer, regardless of its spatial disposition in relation to the OW.

A classic multi-well analysis in homogeneous media consists in plotting OW log-distances versus drawdown at a given pumping time. A straight line is obtained whose slope and vertical offset, respectively, allow estimating spatially averaged values of *T* and *S*, using the Cooper-Jacob model. In non-uniform or heterogeneous media, the points are not expected to form a straight line but rather several lines or curves expressing the successive flow regimes that occurred before the targeted time. The success of such analysis depends on the spatial equilibrium of the current drawdown regime over the entire aquifer. Any target time into transitional stages between two spatially homogenous drawdown regimes may not be likely to produce interpretable plots; hence, late-times are preferred, which more probably correspond to such equilibrium states, and investigate a larger volume of aquifer. Figure 8b displays the distance-drawdown plot for 100 OW placed around the well at distances ranging from 0.1 to 300 m, along eight directional axes (Fig. 8b). OW located along the Ox axis are symbolized by circles (east side) and crosses (west side). Drawdowns at these OW clearly exhibit two straight lines, with slopes changing abruptly (western OW) or gradually (eastern OW). Such responses are in accordance with the multi-well derivative analysis depicted above, where eastern OW flow regimes gradually evolve from the first to the second radial flow regime, while western ones display a short transition. These two straight lines depict the two successive flow regimes occurring during the well test, induced by the coexistence of two flow domains. Using the Cooper-Jacob equation $K = 2.3Q/2\pi p$, where p is the slope, one can estimate the apparent conductivity K_{app2} which is equal to $(K_{mA} + K_{mB})/2$. OW located along other directional axes than Ox

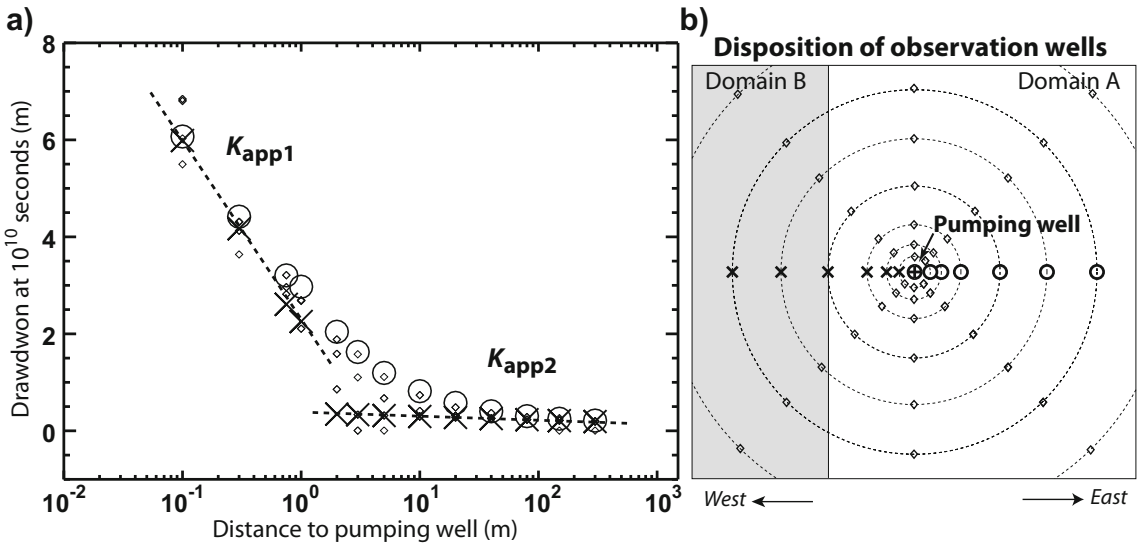

Fig. 8 **a** Distance-drawdown plot. Observation well drawdowns are obtained from flow simulation in the unfaulted leaky case. The simulation parameters are the same as those explained in Figure 6. **b** Spatial arrangement of observation wells

display drawdown levels with intermediate behaviours, i.e., ranging between the two lines formed by Ox-directed western and eastern OW drawdowns.

This distance-drawdown plot is a useful tool to diagnose the presence of two laterally contiguous flow domains, when two straight lines are exhibited either with a gradual or abrupt change. It provides valuable insight, along with the derivative and flow dimensional analysis, allowing for confident interpretation of this conceptual model.

Contiguous aquifers with faulted interface

Rafini and Larocque (2009) proposed an interpretative model for aquifers crosscut by a steeply inclined conductive fault that is not directly connected to the well. These results corroborated the analytical model proposed by Abbaszadeh and Cinco-Ley (1995) and provided the flow dimension diagnostic signature (2 – 4 – 1.5 – 2). This signature indicates the following chronological succession of flow regimes: (1) an early radial flow before the fault is reached, with a plateau elevation equal to $2.3Q/4\pi T_m$, where T_m is the embedding aquifer transmissivity; (2) a characteristic transitional regime $n = 4$; (3) the $n = 1.5$ typical fractional response of a conductive fault (also referred to as bilinear); and (4) a late radial flow regime that is identical to the early radial flow, during which the fault no longer influences the aquifer (Rafini and Larocque 2009). At this late radial stage, the aquifer response is controlled only by the hydraulic properties of the embedding aquifer, and the fault becomes transparent. In this model, the fact that early and late radial stages are identical (in other words, that their plateau elevations are equal) is a key point that indicates that flow domains on both sides of the fault are identical and that the fault does not juxtapose two distinct lithological units. Here, the study numerically investigates the case in which the fault embodies the interface between two distinct hydraulic blocks. The parameters of the numerical simulation are analogous to that described in the previous section in all aspects, except for the presence of a third hydraulic unit (the fault), which is much thinner and located between the two domains (Fig. 1). The simulation strategy is also analogous to the one explained previously, wherein a series of sensitivity analyses are performed to independently identify the respective impacts of each hydraulic parameter or combinations of parameters on the macroscopic response recorded at the pumping well.

The drawdown response obtained at the pumping well is presented in Fig. 9, in the form of a sensitivity analysis of coupled K_{mB} and S_{s_mB}. These parameters are progressively modified by steps of half an order of magnitude, which increase and decrease from the equality to domain A properties (dotted curve). Modifying these parameters in the same way was set for illustrative purposes, to keep the domain B diffusivity $\eta_{mB} = K_{mB}/S_{s\_mB}$ constant and to optimize the visibility of the successive flow regimes. A succession of four flow regimes marked by flow dimension values 2, 4, 1.5, and 2 is obtained, which is analogous to the succession achieved by Rafini and Larocque (2009) for a single flow domain crosscut by a fault, except that in this case, the early and late radial flow regimes display unequal plateau elevations. These two early and late radial flow regimes are identical to that of the unfaulted model addressed in the previous section. Remarkably, the obtained sequence turns out to be a trivial combination of the respective signatures generated by, respectively, a single conductive fault embedded into an aquifer ($n = 1.5$), and contiguous aquifers with unfaulted interface (n sequence 2 – 4 – 2 with unequal plateau elevations).

Similar to the unfaulted cases, the apparent conductivity calculated from the late radial plateau elevation corresponds to the arithmetic mean of the conductivities for

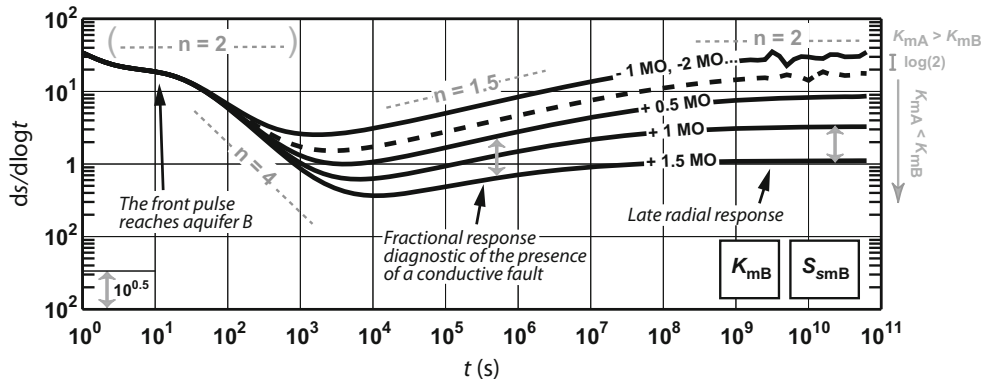

Fig. 9 Drawdown log-derivative response and flow dimension (n) analysis for flow simulations in faulted laterally juxtaposed flow domains. A series of simulations are performed with identical parameters except for the conductivity and specific capacity of the non-pumped domain (K_{mB} and S_{s_mB}, respectively), which vary by the quantity indicated on each signal (*MO* magnitude order), compared with the case in which both domains have equal properties (dotted signal). Other parameters are $K_{mA} = 10^{-7}$ m s^{-1}; $S_{s\_mA} = 10^{-6}$ m^{-1}; $b_m = 42$ m; $K_f = 10^{-3}$ m s^{-1}; $S_{s\_f} = 10^{-5}$ m^{-1}; $b_f = 0.34$ m; and $Q = 4.16 \times 10^{-4}$ m^3 s^{-1}. Noise occurrence in late time is due to numerical instability

domains A and B. Figure 9 illustrates that this elevation inversely and linearly evolves with K_{mB} (as indicated by the gray arrow; the vertical offset is a factor that is equal and inverse to the variation of K_{mB}), when K_{mB} exceeds K_{mA}. When K_{mB} is less than K_{mA}, the elevation of the late radial plateau tends to remain equal to twice the early radial plateau elevation, mimicking the behavior of non-leaky cases described in the previous section. Moreover, the simulations demonstrate that during the preceding $n = 1.5$ flow regime, the vertical offset, a_f, of the log-derivative straight-line response (a_f strictly equals $ds/d\text{-}\log(t)$ at $\log(t) = 0$, see Fig. 10) evolves as an inverse square root function of K_{mB} S_{s_mB} when $K_{mB} > K_{mA}$, as visible in Fig. 9. Hence, $a_f \sim (K_{mB}\ S_{s\_mB})^{-0.25}$. The effects of other hydraulic parameters, such as K_{mA}, S_{s_mA}, T_f, S_f, b and Q, on a_f were analysed, leading to Eq. (3) (Table 1). The simulations are also designed to identify eventual non-independent factors, which would express in the equation through the presence of additive or subtractive operators. The only additive operator is K_{mB}+ K_{mA}. This factor does not modify the effect of other parameters because it is situated at the downstream end of the hierarchical structure of the equation. Finally, this equation is analogous in its form to the general equation of aquifers crosscut by a steeply inclined conductive fault (Rafini and Larocque 2009, 2012).

The time, t_{2AB}, which marks the transition between the fractional and late radial flow regimes (Fig. 10), can be derived using the a_{r2} and a_f equations displayed in Table 1 (Eqs. 2 and 3). Thus, a graphical interpretation of a_f and t_{2AB} makes it possible to calculate the fault transmissivity, T_f, and the apparent specific storage of the embedding aquifer, S_{s_m}, using Eqs. (3) and (7), after having previously derived the apparent transmissivity of the embedding aquifer, 0.5 ($T_{mA} + T_{mB}$) from the interpretation of a_{r2} using Eq. (2).

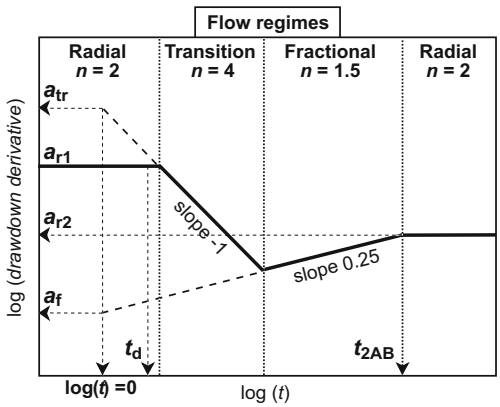

Fig. 10 Schematic illustration of the successive flow regimes predicted in the faulted leaky model, and their associated graphical features (see Table 1 for equations)

Discussion

Summary of the conceptual models

The flow dimension sequences obtained are summarized in Fig. 11. The (2 – 2) sequence with non-equal plateau elevations can be interpreted as the presence of two contiguous hydraulic domains with non-equal properties. The positive or negative vertical offset between both plateau elevations indicates whether or not the juxtaposed non-pumped domain is more transmissive than the pumped one. The apparent transmissivity as derived from the late plateau's elevation (Eq. 2) is the arithmetic mean of both aquifers. This result corroborates Barker and Herbert (1982) for "patchy" aquifers, Butler and Liu (1991) for the strip aquifer, and Guo et al. (2012) for linear aquifers. The $n = 1.5$ segment between the two plateaus indicates that the interface between aquifers is a conductive fault. A graph of various segments' intercepts and intersection times leads to the estimation of the hydraulic properties of the fault and aquifers, using equations displayed in Table 1.

The results interestingly imply that when the non-pumped domain is more transmissive than the pumped domain by one or more orders of magnitude, the large-time response at the pumping well is independent of the pumped domain's hydraulic properties. This also aligns with the conclusions of Barker and Herbert (1982) regarding radial "patchy" aquifers. It is a common belief in applied hydrogeology that "bulk" aquifer properties are obtained by analysing the late rather than early time straight line on drawdown semi-log plots when several straight segments are present with non-equal slopes. Although in a first approach, such bulk properties appear to be representative of reality because they are averaged over an extended volume of depressurized aquifer, in fact, these results show that the bulk properties may actually not describe the targeted aquifer but rather may correspond to a blind, more transmissive hydraulic region which is not intercepted by the borehole. The obtained apparent transmissivity is in actual fact half the real transmissivity of this region.

The contour maps displayed in Fig. 12 make it possible to represent the transient diffusion of the front pulse during the early and mid-time of a pumping test, before and during the non-pumped domain and when the fault begins to exert a significant influence on the general hydrodynamics of the aquifer. For the leaky models (Fig. 12a,b), the non-pumped aquifer predominantly supplying groundwater to the well is visible as the front pulse becomes larger than that of the pumped aquifer, because it diffuses faster. Predictably, in non-leaky models, the non-pumped domain is practically non-depressurized. In both hydraulic configurations, the presence of a conductive fault at the interface leads to a longitudinal drastic extension of the area of influence of the pumping, in such a manner that regions far afield are likely depressurized. If a more greatly transmissive remote area is

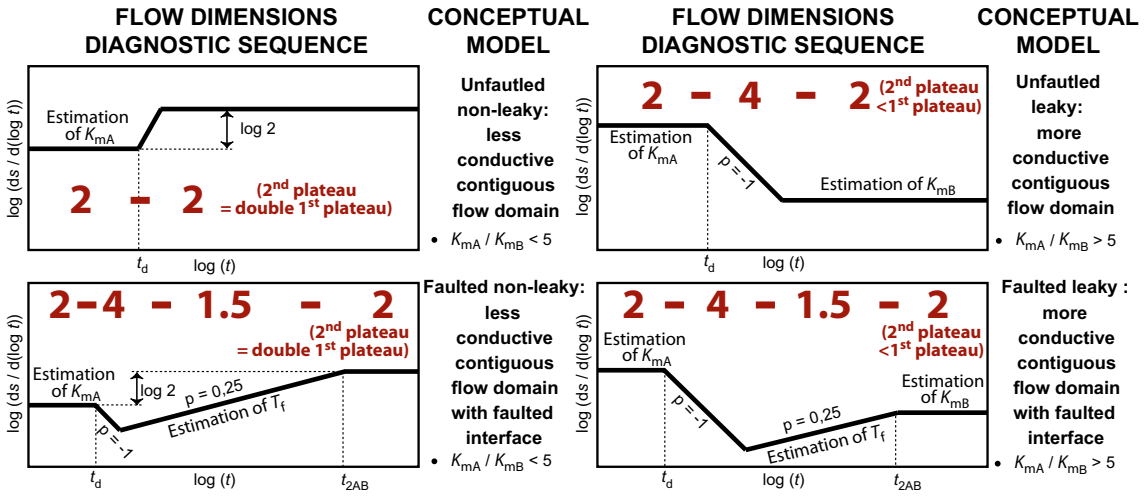

Fig. 11 Summary of the diagnostic flow dimension sequences analyzed in this study (the successive values of flow dimension are indicated in *large bold numbers*) and the associated conceptual models achieved by numerical investigations. Time, t_d, corresponds to the time needed to reach the lateral aquifer

reached by such means, into which the front pulse expands rapidly and becomes dominant, it is likely that the pumping well response will reflect the hydraulic properties of this distant region.

As a general statement, the results indicate that the aquifer response is governed by the region with the highest transmissivity rather than the lowest, contrary to what may be apprehended intuitively. The reason is that the response at the pumping well reflects the expansion of the front pulse. The apparent transmissivity obtained at a given pumping time reflects the region into which the front pulse is currently and predominantly expanding, i.e., the most transmissive region,

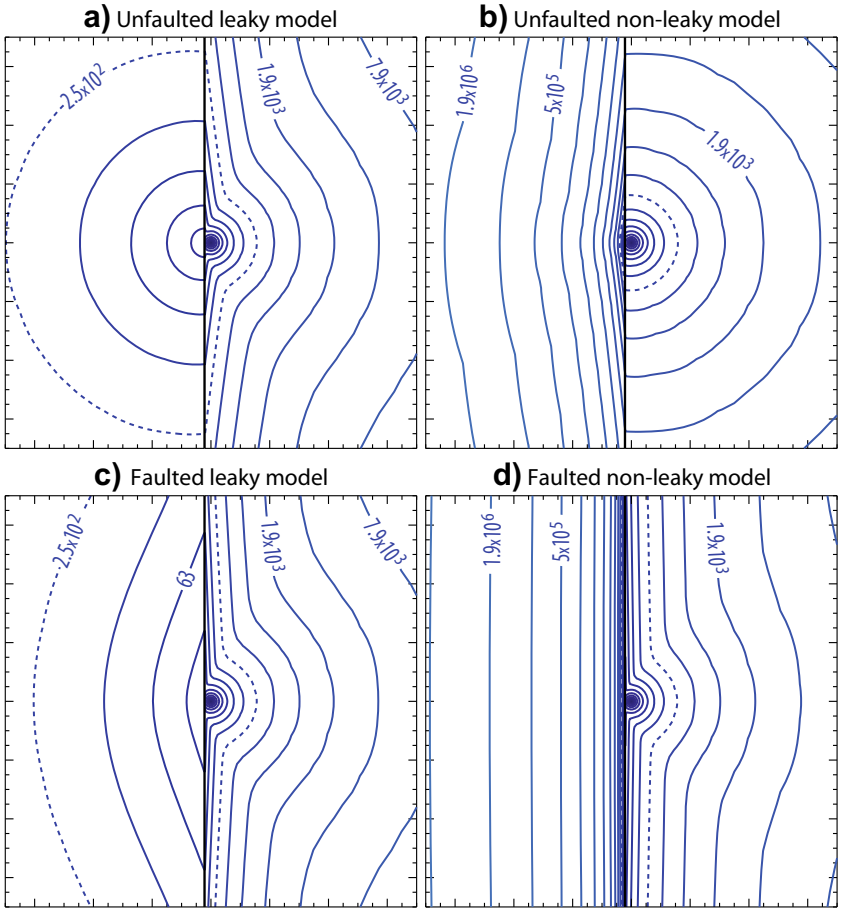

Fig. 12 Front pulse propagation contour maps obtained from simulations. Labels are elapsed pumping time in seconds. The represented area is zoomed in (lateral length is 140 m) on the center of the larger simulated domain; hydraulic boundaries effects are invisible here. The *dotted contour* corresponds to the same time in the four images (2.51×10^2 s). Simulations input values are: $d = 2$ m, $K_{mA} = 10^{-7}$ m s^{-1}; $S_{mA} = S_{mB} = 10^{-5}$ m^{-1}; $S_f = 3.16 \times 10^{-5}$ m^{-1}; **a** and **c** $K_{mB} = 10^{-5}$ m s^{-1}; **b** and **d** $K_{mB} = 10^{-9}$ m s^{-1}; **c** and **d** $K_f = 3.16 \times 10^{-3}$ m s^{-1}; $b_f = 0.34$ m

even if that region is not connected to the pumping well, rather than to regions that were previously spanned by the front pulse.

Practical use of the models

Duration and visibility of the segments

The duration of simulations was intentionally set to be extremely long and the distance between the pumping well and the interface very short, for experimental and illustration purposes. A large number of numerical simulations were performed in order to constrain the models that are presented in Figs. 3 and 10 and in Table 1; the curves displayed in Figs. 2 and 9 are only illustrative examples. Since the influence of each input parameter on the general response has been strictly deciphered, it is very easy to understand the manner with which the resulting theoretical responses are not restricted to the singular combinations of hydraulic parameters of the presented simulation cases. For instance, changing d to 20 m and K_{mA} to 10^{-4} m s^{-1} would produce a strictly identical result to that presented in Fig. 2, for equal K_{mA}/K_{mB} ratios (except, of course, that the early radial plateau would be two log-cycles lower). Similarly, a decrease of T_f by a half order of magnitude causes the late radial plateau to begin one log-cycle earlier, according to the definition of t_{2AB} (see Eq. 7 in Table 1).

The critical duration of one log-cycle has been recommended by Beauheim et al. (2004) for a proper identification of a derivative straight segment prior to the estimation of the associated flow dimension. Using this criterion, it can be seen in Fig. 2 that, for a 3-day-long pumping test, the complete (2 – 4 – 2) sequence is visible for any K_{mA}/K_{mB} ratio greater than 10^{-2}. For a 2-week-long test, this critical ratio is practically 10^{-3}. For shorter tests, or lower K_{mA}/K_{mB} ratios, the late radial stage will not have time to settle before the end of pumping. Similarly, Fig. 9 shows that a two-week long pumping test is necessary to allow for the entire combination of sequences (2 – 4 – 1.5 – 2) to be observed in optimal conditions. This is for the specific combinations of hydraulic parameters shown Figs. 2 and 9; a generalization is provided into the next sections.

The early radial stage will be lacking in cases where a fast diffusion into the pumped aquifer – high η_{mA} – is conjugated with a short distance d between the interface and the pumping well: d^2/η_{mA} is the controlling factor, according to the definition of t_d (see Eq. 5 in Table 1). In real-world conditions where a buffer period of 10^2 s might be considered reasonable to cover pumping rate stabilization and wellbore storage effects, i.e., before the drawdown response actually reflects real aquifer conditions, the settlement of the early radial stage during one log-cycle requires that $t_d = 10^3$ s. Referring to $t_d = (d^2/\eta_{mA})/2.25$, in order for the early radial stage to be visible, the criterion is $d^2/\eta_{mA} \geq 2{,}250$ s. If the pumped aquifer has conductivity K_{mA} as low as 10^{-8} m s^{-1}, and assuming $S_{s\_mA} = 10^{-6}$ (two realistic lower limiting values for confined hard-rock aquifers, e.g., Batu 1998), this brings the minimum distance d_{min} to 4.7 m, while to the contrary, the upper limiting values $K_{mA} = 10^{-3}$ m s^{-1} and $S_{s\_mA} = 10^{-5}$ m^{-1} give $d_{min} =$ 474 m. These constitute realistic distance ranges for real-world settings.

For the unfaulted leaky model, the minimum K_{mA}/K_{mB} ratio for late radial stage to settle one log-cycle during a given pumping test duration, t_{pump}, can be estimated by posing $t_2^* \leq t_{pump}/10$, where t_2^* is the approximated beginning of this radial stage. Following the equation of t_2^* (see Eq. 6 in Table 1), this gives $0.21\ (d^2/\eta_{mA})\ (K_{mB}/K_{mA}) \leq t_{pump}/10$. By considering $d^2/\eta_{mA} = 2{,}250$ s, it can hence be determined that the full (2 – 4 – 2) sequence will be visible for 3-day, 2-week and 3-month-long pumping tests, for any K_{mA}/K_{mB} ratio higher than, respectively, $10^{-1.74}$, $10^{-2.4}$ and $10^{-3.22}$. For non-optimal values of d^2/η_{mA}, these limiting ratios will increase by a factor equal to $d^2/(2{,}250\ \eta_{mA})$. To conclude, the full exhibition of the (2 – 4 – 2) sequence is a realistic forecast in hard-rock aquifer contexts where the conductivity contrast does not exceed two to three orders of magnitude depending of the pump test duration (3 days to 3 months), for optimal values of d^2/η_{mA}. However, the latter ratio may constitute a more restrictive control on the full observation of the sequence. A valuable insight is that, for tests that last 3 days or less, the response (2 – 4) is predicted where K_{mA} is low and d is high, for almost all conductivity log-ratios greater than 1.5. These results cause one to question the universal interpretation of the (2 – 4) sequence as a recharge boundary in short- and medium-term pump tests.

For the faulted leaky model, the experiment revealed that the starting time, t_{2AB}, of the late radial stage evolves with the ratio $T_f^2/(K_{mA} + K_{mB})^3$, as depicted in Eq. (7) (Table 1). A consequence is that a very high conductivity of the fault or a low conductivity of embedding aquifers will tend to delay the settlement of this radial stage. It will be exhibited over one log-cycle at the end of a pumping test of duration t_{pump} if $t_{2AB} < t_{pump}/10$, hence $T_f^2/K_m^3 \leq 5.6 \times 10^{-2}\ t_{pump}/S_{s\_m}$, according to Eq. (7). For the sake of simplicity, the terms K_m and S_{s_m} are used, which are the properties of the most conductive embedding aquifers (an acceptable first-order approximation thus is $K_m = 2 \times K_{app}$). Assuming $S_{s\_m} = 10^{-5}$ m^{-1} and $t_{pump} = 1.2 \times 10^6$ s (2 weeks), this leads to $T_f^2/K_m^3 \leq 6.7 \times 10^9$. In other words, the late radial stage will be visible within 2 weeks in real-world cases where the contrast between the fault transmissivity and the conductivity of the most conductive embedding aquifer is not drastic, namely if $\log (T_f/K_m^{1.5}) \leq 2.4 + 0.5 \log (S_{s\_m})$. Moreover, according to previous results (Rafini 2008; Rafini and Larocque 2009), the occurrence of $n = 1.5$ fractional flow is directly governed by the diffusivity ratios η_f/η_m: it is forecast for any value of this ratio greater than 1 and a first-order approximation of its log-duration is given by the square of this ratio. Furthermore, these authors achieved Eq. (8) (Table 1) for the beginning time, t_1,

representing the diffusion slow-down into the fault, a necessary condition for the $n = 1.5$ flow regime to occur. Hence, this regime will exhibit over one log-cycle if the two following conditions are met: (1) the regime begins before $t_{pump}/10^2$; i.e., $t_1 \leq t_{pump}/10^2$ which gives $11\ S_f{}^2/(K_m\ S_{s\_m}) \leq t_{pump}$, and hence $K_m \geq (11/t_{pump})\ (S_f{}^2/S_{s\_m})$; and (2) the regime lasts at least one log-cycle, i.e., $\eta_f/\eta_m \geq 10^{0.5}$, hence $T_f/K_m \geq 10^{0.5}\ S_f/S_{s\_m}$. To set ideas, assuming $S_{s\_m} = 10^{-5}\ m^{-1}$, $S_f = 5 \times 10^{-5}$ (as fault-rock typically is slightly more compressible than sound rock) and $t_{pump} = 1.2 \times 10^6$ s (2 weeks), the $n = 1.5$ stage will be visible if $K_m \geq 2.3 \times 10^{-9}\ m\ s^{-1}$ and $T_f/K_m \geq 15.8$, both of which are highly plausible conditions. Going further, combining these criterions with that depicted above for the occurrence of the late radial stage leads to the following conditions of exhibition for the (1.5 – 2) sequence: $K_m \geq 2.3 \times 10^{-10}\ m\ s^{-1}$, $T_f/K_m \geq 15.8$ and $T_f{}^2/K_m{}^3 \leq 6.8 \times 10^9$. These constitute non-restrictive conditions towards the model's validity in the real world. Ultimately, for the complete (2 – 4 – 1.5 – 2) sequence, all these criterions must be verified, along with some temporal constraints on the distribution and visibility of the four successive segments into realistic pump test timelines. Taking the minimum, $t_d = 1{,}000$ s, for the early radial stage to settle (see the preceding), plus one log-cycle for each segment, gives 10^7 s (3.7 months). Adding the transition time-periods leads to unrealistically long times. A consequence is that this sequence will likely occur in real-world conditions in a truncated form: the early and/or the late radial stage will be partially visible or even lacking. Also, the $n = 4$ or $n = 1.5$ segments will atrophy under some combinations of hydraulic parameters—for instance, it is shown here that the log-duration of the $n = 4$ segment is a condition of the ratio $K_{mB}{}^{0.2}/K_{mA}{}^{0.6}$, as well as the product $(K_{mB}\ T_f)^{0.2}$. In contrast, the $n = 1.5$ segment's log-duration is a function of $(\eta_f/\eta_m)^2$, as obtained by posing t_{2AB}/t_1, where the subscript m refers to the most conductive aquifer (which must be K_{mB} concerning the 4 – 1.5 sequence). The $n = 1.5$ segment's duration is thus independent of the ratios between aquifers properties, and rapidly decreases with K_{mB}, in contrast with the $n = 4$ segment. Hence, the respective durations of the mid-time segments $n = 4$ and $n = 1.5$ both increase with T_f but exhibit opposite relationships on K_{mB}.

To conclude, these considerations demonstrate that the submitted models are plausible and suitable to the timelines of real-world pumping tests under wide and realistic ranges of hydraulic properties, except the full four-segment sequence that rather likely occurs in truncated form as explained. However, where only partial sequences are obtained that are (2 – 4 – 1.5), (1.5 – 2), (4 – 1.5 – 2), (2 – 4), (4 – 2), or eventually (4 – 1.5), incomplete, yet highly valuable, interpretations may still be conducted. The (1.5 – 2) sequence by itself makes it possible to interpret a conductive fault embedded into an aquifer, and the calculation of the hydraulic properties of both the aquifer and the fault. The (4 – 1.5) sequence alone makes it possible to qualitatively identify that such a conductive fault is not directly connected to the wellbore, yet T_{mB} and T_f can be quantified only if the late radial plateau is visible, leading to the sequence (4 – 1.5 – 2). The sequence (4 – 2) is sufficient to interpret the presence of a non-pumped, blind and highly transmissive flow domain, and T_{mB} can be quantified. The (2 – 4) sequence points to the presence of a more transmissive, non-pumped aquifer, unless a recharge boundary is observed in the environment.

Impact of the geometrical assumptions

Where the model's basic postulates are verified in nature, pumping tests will render the predicted responses, under the conditions depicted in the previous section; however, the model is geometrically idealized. This section deciphers the impact of the two main geometrical assumptions of the model: (1) the interface's verticality, and (2) the equality of lower boundaries for the fault and surrounding aquifers. Before everything else, it should be noted that these are classical assumptions of fault-aquifer flow models (Gringarten et al. 1974; Cinco-Ley and Samaniego 1981; Abbaszadeh and Cinco-Ley 1995; Rafini and Larocque 2009). Both a slight inclination of the interface, either faulted or not, and a fault whose bottom is significantly deeper than embedding aquifers, would be reflected by an additional time-period during which the diffusion into the fault and/or aquifer B is not strictly horizontal, that is, before the front pulse diffusion reaches the top and bottom boundaries and practically reverts to the horizontal. For a faulted interface, Rafini and Larocque (2012) demonstrated that the drawdown response associated with such a flow regime is a fault-related radial stage prior to settlement of the $n = 1.5$ flow regime. For the non-faulted leaky model, a spherical regime prior to the late radial stage is expected. In both cases, this would tend to delay the beginning of the subsequent flow regimes. However, this delay is only significant if: (1) the interface's inclination is low (which is outside the scope of this study); (2) the root of the fault is greatly deeper than the substratum of surrounding aquifers; or (3) the diffusivity of the fault or of aquifer B is very low, leading to the late radial stage being controlled by aquifer A properties only, since the interface acts as a no-flow boundary. To conclude, the submitted models remain valid when the assumption of the interface's verticality is only partially verified or when the fault's thickness is moderately greater than the thickness of the aquifer. The models are not intended to be applied to configurations with highly inclined interfaces or high contrasts between fault and aquifer thickness. Such cases generate 3D flow with flow regimes that are not accounted for in this study, namely fault-related radial flow and spherical flow. Finally, cases where the transmissivity change between both flow domains is gradual have been assessed by Levitan and Crawford (1995) for radially symmetric systems. This

essentially results in a more progressive and prolonged transitional stage between both plateaux.

Data quality

It is a common statement that the quality and objectivity of derivative analysis are highly dependent on data quality. In the real world, the derivative diagnostic sequence may be only partly visible or too noisy, making it difficult to properly interpret the conceptual model. Noise may be due either to a significant diffuse random heterogeneity field, or to human errors such as pumping rate instabilities or imprecise measurement. Gaussian noise may be substantially reduced by using specifically designed differentiation algorithms (e.g., Bourdet et al. 1989; Spane and Wurstner 1993). Conversely, sudden changes in pumping rate will be increased by differentiation process since it will be felt over the entire smoothing interval, producing a signal distortion. To conclude, it is recommended that the time-segmentation into successive flow regimes should be performed manually, by simultaneously fitting semi-log drawdown plots, derivative bilog plots and differentiated derivative bilog plots. This makes it possible to properly discriminate between the signal and various forms of noise, and to distinguish between transitional stages and settled flow regimes—a particularly sensitive task. In a second methodological step, the estimation of the flow dimension (or slope) in each segment can be optimized using automated linear regression functions. The use of any polynomial regression function, by its very nature, is not suitable to the approach promoted by this study.

Uniqueness of interpretations

It is well recognized that derivative data are much more sensitive to hydraulic conditions than drawdown only (e.g., Issaka and Ambastha 1999; Samani et al. 2006), allowing for finer and more objective aquifer interpretations. Still, in some cases, the differences between theoretical responses may be very subtle and hardly visible from real data, in such manner that several conceptual models may be attributed to a single dataset. This long-debated issue of non-uniqueness remains the largest difficulty in interpreting pumping tests. It may be overcome by providing subsidiary, often geological, inputs on hydraulic conditions. A great advantage of hydrogeological analysis over petroleum research still lies in the common use of observation-well responses. The numerical experiment reported here demonstrates that multi-well analysis provides spatial insights that may be highly valuable in adequately identifying the proposed conceptual model. Two plots proved useful in doing so: derivative responses of observation wells versus time, eventually using a standard Cooper-Jacob time-normalization by r^2, and distance-drawdown plots where the interpretation of two distinct straight segments is indicative of two successive radial flow regimes.

Derivative data displaying two successive radial plateaux have been predicted by other conceptual models: dual porosity (Warren and Root 1963; Boulton and Streltsova 1977; Moench 1984), unconfined aquifer (Moench 1997), and "T" shape aquifers (Dewandel et al. 2014). It is worth noting that the differences between these theoretical responses lie in the shape of the transitional stage between the plateaux. The dual porosity derivative response forms a characteristic "V" depression between both plateaux, which is deeper in models with a pseudo-permanent rather than transient transfer function between matrix and fractured continua (e.g., Bourdet et al. 1989). Such a feature is totally absent from predicted responses produced by juxtaposed flow domains, providing a means of discrimination between these conceptual models. The "T" shape aquifer described by Dewandel et al. (2014) addresses cases where two symmetrical lateral domains are less conductive and shallower than a central and deep pumped domain, representing a vertical, deep-rooted, fault-unit crosscutting a more surficial hardrock aquifer. Such a configuration exhibits a close analogy to the non-leaky case analysed in the present study. The present study's results corroborate the Dewandel et al. model, in that two successive radial plateaux are obtained, the late being systematically higher than the early plateau, their respective elevations being governed by the transmissivities of flow domains, and the storativity ratio exerting a more limited influence and essentially impacting the transitional stage. However, one submits that, since the late-time apparent transmissivity is an average of the transmissivities of both domains, transmissivity ratios of ten or greater produce drawdown regimes at the pumping well that are practically not impacted by the lower transmissivity value, whether this value originates from the pumped or the non-pumped domain (Figs. 2, 3 and 4). It is therefore observed that (1) when the non-pumped aquifer is less transmissive by a factor of 10 or more than the pumped one, it has an influence on the pumping well response similar to that of an impermeable barrier (i.e., doubling the drawdown rate); and (2) the impermeable barrier constitutes a limiting case and thus the elevation of the second plateau must theoretically not exceed double that of the first plateau, under any conditions. Finally, the "T" shape model postulates that the faults generate a radial stabilization rather than an $n = 1.5$-fractional-flow regime. From a conceptual standpoint, this may relate to the wide transversal extent of the fault, and to the highly contrasted depth ratio between the pumped domain (in this case, the fault) and non-pumped domains—a statement whose validation would require 3D simulation. These two criteria could hence be adjustment variables between the two conceptual models of faulted aquifers.

Finally, the conclusions corroborate those of Butler and Liu (1991) in that a segmented response is predicted with the early radial flow regime relating to the flow domain which is directly connected to the pumping well, while later regimes, radial

and non-radial, mark the predominant influence of successive juxtaposed flow domains on the aquifer's response, as the front pulse propagates. Similar to the numerical results with faulted aquifers found for this study, the semi-analytical approach of Butler and Liu predicts a fractional $n = 1.5$ stage when the strip is drastically more transmissive than surrounding domains. The strip indeed begins behaving like a fault when the pressure diffusion inside it is linear and exerts a dominant control over the geometry of the depressurization front into the adjacent matrix domain (see Rafini and Larocque 2009). In other words, the strip must be depressurized over its entire transversal extent, which implies an additional transitional time-period that delays the settlement of the fractional regime. Such a strip must therefore have a very short transversal extent and be extremely diffusive for the fractional stage to occur, unless it is situated very close to a pumping well.

Conclusions

This technical note numerically investigates the transient hydraulic behavior of the archetype aquifer model composed of two laterally juxtaposed flow domains with non-equal properties, with or without a conductive fault at the interface. The study focussed specifically on the flow-dimensional sequence occurring during constant-rate pumping tests. An interpretative framework is developed that provides valuable insights into the identification of such heterogeneous flow conditions. A critical emphasis was placed on the real-world conditions of application of the model, and on its unicity. It is also explained how multi-well datasets may be used to interpret the proposed model with greater confidence.

Key results are:

1. Two radial flow stages are predicted that correspond to the periods before and after the moment when the non-pumped aquifer is reached; with an optional transitional stage marked by a flow dimension equal to 4 (negative unit slope of the derivative signal).
2. The apparent transmissivity calculated from the second radial plateau is equal to the arithmetic mean of the transmissivity of both aquifers. Hence, for transmissivity ratios practically greater than ten, the least transmissive aquifer does not exert a significant influence on the drawdown response at the pumping well, however the apparent transmissivity is half the higher one.
3. When the non-pumped aquifer is less transmissive than the pumped aquifer, its influence tends to be similar to that of an impermeable barrier (the drawdown rate is doubled), a limiting behavior that occurs beyond transmissivity ratios as small as ten.
4. In contrast, when the non-pumped domain is more transmissive than the pumped domain (practically, more than ten times), the aquifer's general late-time response is exclusively controlled by the depressurization of the non-pumped domain.
5. This implies a counterintuitive observation to the effect that when two straight segments are visible on time-drawdown semi-log plots, the apparent transmissivity given by the late segment does not correspond to a bulk transmissivity of the region that is physically investigated but rather to that of a distant, blind, non-pumped region.
6. In such a case, the depressurization of the non-pumped aquifer induces a sudden decrease of the drawdown rate at the pumping well that may be misinterpreted as a recharge frontier when using an inappropriate interpretative methodology.
7. A valuable input for confidently interpreting the promoted conceptual model lies in multi-well distance-drawdown plots that characteristically exhibit two straight lines with either an abrupt or a gradual transition, depending on the orientation of the observation well in relation to the interface.
8. Going further, transmissivity values measured from late-time stabilizations of the drawdown log-derivative at observation wells (OW) likely corresponds to that of the most transmissive region of the aquifer, whether or not it encompasses the OW; this invalidates the common postulate that OW strictly investigates the hydraulic properties of the area between the OW and the pumping well.
9. The existence of a conductive fault at the interface between both flow domains produces a characteristic intermediate segment with flow dimension equal to 1.5, whose duration is proportional to the square diffusivity ratio between the fault and the most transmissive embedding aquifer.
10. Because a conductive fault induces fast and expanded pressure diffusion along its longitudinal axis, it is capable of provoking the depressurization of remote transmissive regions in such manner that the aquifer which predominantly supplies groundwater to the pumping well—and which governs the late radial flow regime—is distant from the targeted site of investigation.
11. It is shown that the obtained responses are predicted for a wide range of realistic combinations of hydraulic parameters; however, where the flow dimension sequence is longer than the pump test, even a partial exhibition that leads to an incomplete analysis may yet be valuable. In particular, a partial exhibition is forecast in the case of a transmissive non-pumped aquifer, where the contrast in transmissivity exceeds three orders of magnitude due to an extended-duration transition segment $n = 4$, and where the interface is a conductive fault, as the predicted full sequence is very long (2 – 4 – 1.5 – 2).

From a practical standpoint, this study proposes several recommendations for the interpretation of pumping tests where drawdown responses display several straight segments on semi-log plots. This work provides a general methodological framework to understand such responses, by deciphering the relationships between the apparent hydraulic properties calculated from respective segments, and the real properties of distinct hydraulic regions of the heterogeneous aquifer. In addition, the method proposed in this study makes it possible to identify the existence of a conductive fault at the interface between two regions with non-equal transmissivities, based on the analysis of the drawdown response at the pumping well and, optionally, at observation wells.

When appropriately applied, the methodology described in this technical note can be used to better interpret aquifer responses to pumping. It is hoped that this method be considered when testing heterogeneous aquifers that exhibit various and unfamiliar hydraulic behaviors, which will avoid errors caused by the use of conventional methods, provide a better diagnostic of the pumping test and improve heterogeneous aquifer assessments.

Acknowledgements The authors would like to thank the National Sciences and Engineering Research Council of Canada (NSERC - individual discovery grants program) and the Fonds de recherche du Québec - Nature et technologies (FRQNT- new university researchers start-up program) grant programs held by Prof. Romain Chesnaux for their financial contribution in supporting this study. The manuscript benefited from fruitful review by R. Beauheim and an anonymous associate editor. The manuscript was kindly checked by Josée Kaufmann.

References

Abbaszadeh M, Cinco-Ley H (1995) Pressure-transient behavior in a reservoir with a finite-conductivity fault. SPE Form Eval 10:26–32. doi:10.2118/24704-PA

Avci CB, Şahin AU, Çiftçi E (2013) A new method for aquifer system identification and parameter estimation. Hydrol Process 27:2485–2497. doi:10.1002/hyp.9352

Ambastha AK (1989) Pressure transient analysis for composite systems. DOE/BC/14126-11, SUPRI TR 68, US Department of Energy, Washington, DC, 178 pp

Ambastha AK, McLeroy PG, Sageev A (1989) Effects of a partially communicating fault in a composite reservoir on transient pressure testing. SPE Form Eval 4(2):210–218

Batu V (1998) Aquifer hydraulics: a comprehensive guide to hydrogeologic data analysis. Wiley, New York, 727 pp

Banton O, Bangoy L (1999) Hydrogeologie: multiscience environnementale des eaux souterraines [Hydrogeology: environmental multidisciplinary study of groundwater]. Presse de l'Université du Québec, AUPELF-UREF, Sainte-Foy, QB

Barker J (1988) A generalized radial flow model for hydraulic tests in fractured rock. Water Resour Res 24:1796–1804. doi:10.1029/WR024i010p01796

Barker JA, Herbert R (1982) Pumping tests in patchy aquifers. Groundwater 12(2):150–155

Beauheim RL, Roberts RM, Avis JD (2004) Well testing in fractured media: flow dimensions and diagnostic plots. J Hydraul Res 42:69–76. doi:10.1080/00221680409500049

Boulton NS, Streltsova TD (1977) Unsteady flow to a pumped well in a two-layered water-bearing formation. J Hydrol 35(3–4):245–256

Bourdet D (2002) Well test analysis: the use of advanced interpretation models, In: Handbook of petroleum exploration and production, Elsevier, Amsterdam, 439 pp

Bourdet D, Ayoub JA, Pirard YM (1989) Use of pressure derivative in well test interpretation. SPE Form Eval 4:293–302. doi:10.2118/12777-PA

Bourdet D, Whittle T, Douglas A, Picard Y (1983) A new set of types curves simplifies well test analysis. World Oil 196:95–106

Brunner P, Simmons CT (2012) HydroGeoSphere: a fully integrated, physically based hydrological model. Groundwater 50(2):170–176

Butler JJ Jr (1988) Pumping tests in nonuniform aquifers: the radially symmetric case. J Hydrol 101:15–30

Butler JJ, Liu WZ (1991) Pumping tests in non-uniform aquifers: the linear strip case. J Hydrol 128:69–99

Cello PA, Walker DD, Valocchi AJ, Loftis B (2009) Flow dimension and anomalous diffusion of aquifer tests in fracture Networks. Vadose Zone J 8(1):258–268. doi:10.2136/vzj2008.0040

Chesnaux R, Rafini S, Elliott AP (2012) A numerical investigation to illustrate the consequences of hydraulic connections between granular and fractured-rock aquifers. Hydrogeol J 20:1669–1680. doi:10.1007/s10040-012-0912-9

Cooper HH Jr, Jacob CE (1946) A generalized graphical method for evaluating formation constants and summarizing well-field history. Trans Am Geophys Union 27:526–534. doi:10.1029/TR027i004p00526

Cinco-Ley H, Samaniego F (1981) Transient pressure analysis for fractured wells. J Petrol Techn 33:1749–1766

Dewandel B, Lachassagne P, Zaidi FK, Chandra S (2011) A conceptual hydrodynamic model of a geological discontinuity in hard rock aquifers: example of a quartz reef in granitic terrain in South India. J Hydrol 405:474–487. doi:10.1016/j.jhydrol.2011.05.050

Dewandel B, Aunay B, Maréchal JC, Roques C, Bour O, Mougin B (2014) Aquilina C (2014) Analytical solutions for analysing pumping tests in a sub-vertical and anisotropic fault zone draining shallow aquifers. J Hydrol 509:115–131

Fenske PR (1984) Unsteady drawdown in the presence of a linear discontinuity. In: Rosenshein JS, Bennett GD (eds) Water Resources Monograph. American Geophysical Union, Washington, DC, pp 125–145

Ferris J (1949) Ground water. In: Hydrology. Wiley, New York, pp 198–272

Gringarten AC, Henry J, Ramey HJ, Raghavan R (1974) Unsteady state pressure distributions created by a well in a well with single infinite conductivity vertical fracture. SPE J 14:347–360

Guo JJ, Zhang LH, Wang HT, Qi-Guo L (2012) Well responses in three-zone linear composite dual-porosity reservoirs, In: Zheng J-H (ed) Hydrodynamics: theory and model. InTech, Rijeka, Croatia

Hammond PA, Field MS (2014) A reinterpretation of historic aquifer tests of two hydraulically fractured wells by application of inverse analysis, derivative analysis, and diagnostic plots. J Water Resour Prot 06:481–506. doi:10.4236/jwarp.2014.65048

Hantush MS (1960) Modification of the theory of leaky aquifers. J Geophys Res 65:3713–3725. doi:10.1029/JZ065i011p03713

Issaka MB, Ambastha AK (1999) A generalized pressure derivative analysis for composite reservoirs. J Can Pet Technol 38(16):96–115

Jordan CL, Mattar L (2000) Comparison of pressure transient behaviour of composite and multi-layer reservoirs. Paper 2000-45, Canadian International Petroleum Conference, Calgary, AB, 4–8 June 2000

Levitan MM, Crawford GF (1995) General heterogeneous radial and linear models for well test analysis. SPE paper 30554, 70th Annual Fall Meeting, Dallas, TX, Oct 1995

Meier PM, Carrera J, Sanchez-Vila X (1998) An evaluation of Jacob's method for the interpretation of pumping tests in heterogeneous formations. Water Resour Res 34(5):1011–1025

Moench AF (1997) Flow to a well of finite diameter in a homogeneous, anisotropic water table aquifer. Water Resour Res 33:1397–1407. doi:10.1029/97WR00651

Moench AF (1984) Double-porosity models for a fissured groundwater reservoir with fracture skin. Water Resour Res 20:831–846. doi:10.1029/WR020i007p00831

Oliver DS (1990) The averaging process in permeability estimation from well-test data. SPE paper 19845. SPE Form Eval 5(3):319–324

Oliver DS (1993) The influence of nonuniform transmissivity and storativity on drawdown. Water Resour Res 29(1):169–178

Pechstein A, Attinger S, Krieg R, Copty NK (2016) Estimating transmissivity from single-well pumping tests in heterogeneous aquifers. Water Resour Res 52:495–510. doi:10.1002/2015WR017845

Rafini S (2008) Comportement hydraulique des milieux faillés [The hydraulic behaviour of faulted media]. PhD Thesis, Université du Québec à Montréal, Canada

Rafini S, Larocque M (2009) Insights from numerical modeling on the hydrodynamics of non-radial flow in faulted media. Adv Water Resour 32:1170–1179. doi:10.1016/j.advwatres.2009.03.009

Rafini S, Larocque M (2012) Numerical modeling of the hydraulic signatures of horizontal and inclined faults. Hydrogeol J 20:337–350. doi:10.1007/s10040-011-0812-4

Renard P (2005) The future of hydraulic tests. Hydrogeol J 13:259–262. doi:10.1007/s10040-004-0406-5

Renard P, Glenz D, Mejias M (2008) Understanding diagnostic plots for well-test interpretation. Hydrogeol J 17:589–600. doi:10.1007/s10040-008-0392-0

Roberts RM, Ruskauff GJ, Avis JD (1996) A generalized method for analyzing well tests in complex flow systems. SPE-36023, Petroleum Computer Conference, Dallas, TX, 2–5 June 1996

Rushton KR (2003) Groundwater hydrology: conceptual and computational models. Wiley, Chichester, UK, 433 pp

Samani N, Pasandi M, Barry D (2006) Characterizing a heterogeneous aquifer by derivative analysis of pumping and recovery test data. J Geol Soc Iran 1:29–41

Spane FA (1993) Selected hydraulic test analysis techniques for constant-rate discharge tests. PNL-8539, Pacific Northwest Laboratory, Richland, WA

Spane FA, Wurstner SK (1993) DERIV: a computer program for calculating pressure derivatives for use in hydraulic test analysis. Ground Water 31:814–822. doi:10.1111/j.1745-6584.1993.tb00855.x

Sun X, Xu Y, Lin L (2015) The diagnostic plot analysis of artesian aquifers with case studies in Table Mountain Group of South Africa. Hydrogeol J 23:567–579. doi:10.1007/s10040-014-1203-4

Theis CV (1935) The relation between the lowering of the piezometric surface and the rate and duration of discharge of a well using ground-water storage. Trans Am Geophys Union 16:519–524. doi:10.1029/TR016i002p00519

Tiab D, Kumar A (1980) Application of the p'D function to interference analysis. J Pet Technol 32:1465–1470. doi:10.2118/6053-PA

Verweij JM (1995) Analysis of pumping test data from hard rock aquifers. Report GG R-95-39(A), TNO Institute of Applied Geoscience, Delft, The Netherlands, 62 pp

Warren JE, Root PJ (1963) The behavior of naturally fractured reservoirs. Soc Pet Eng J 3:245–255. doi:10.2118/426-PA

Xiao L, Xu Y (2014) Diagnostic analysis of pumping tests using derivative of dlgs/dlgt with case study. Groundwater. doi:10.1111/gwat.12175